Cell Reports, Volume *41*

Supplemental information

Recruited monocytes/macrophages drive pulmonary neutrophilic inflammation and irreversible lung tissue remodeling in cystic fibrosis

Hasan H. Öz, Ee-Chun Cheng, Caterina Di Pietro, Toma Tebaldi, Giulia Biancon, Caroline Zeiss, Ping-Xia Zhang, Pamela H. Huang, Sofia S. Esquibies, Clemente J. Britto, Jonas C. Schupp, Thomas S. Murray, Stephanie Halene, Diane S. Krause, Marie E. Egan, and Emanuela M. Bruscia

Supplementary Figure S1

A

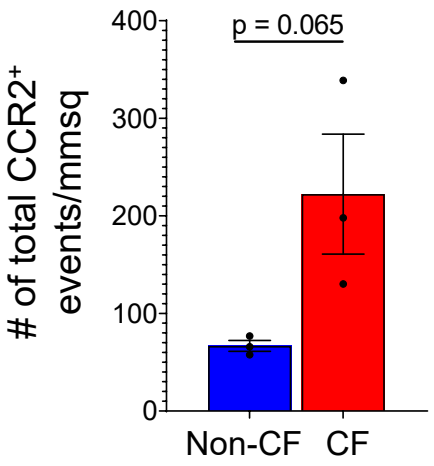

B

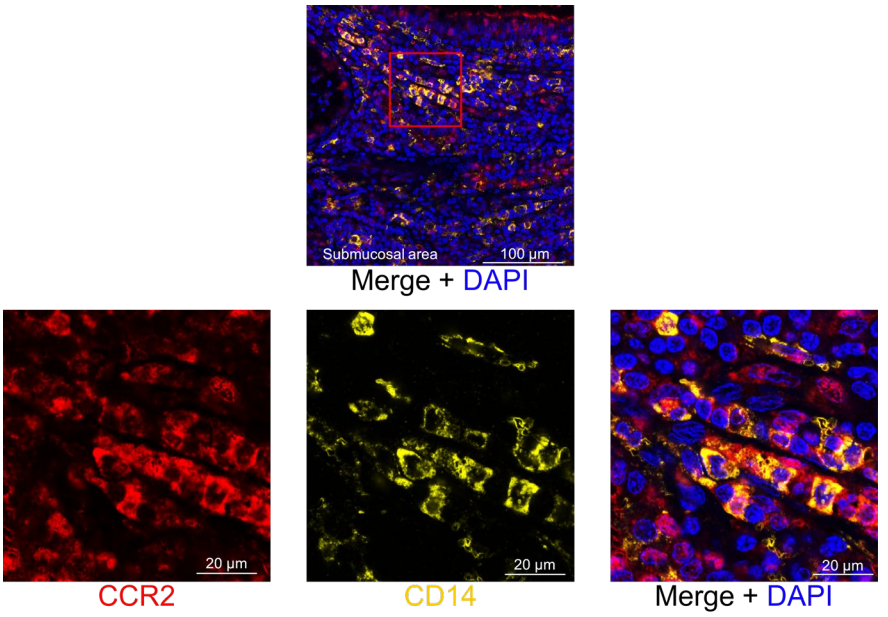

C

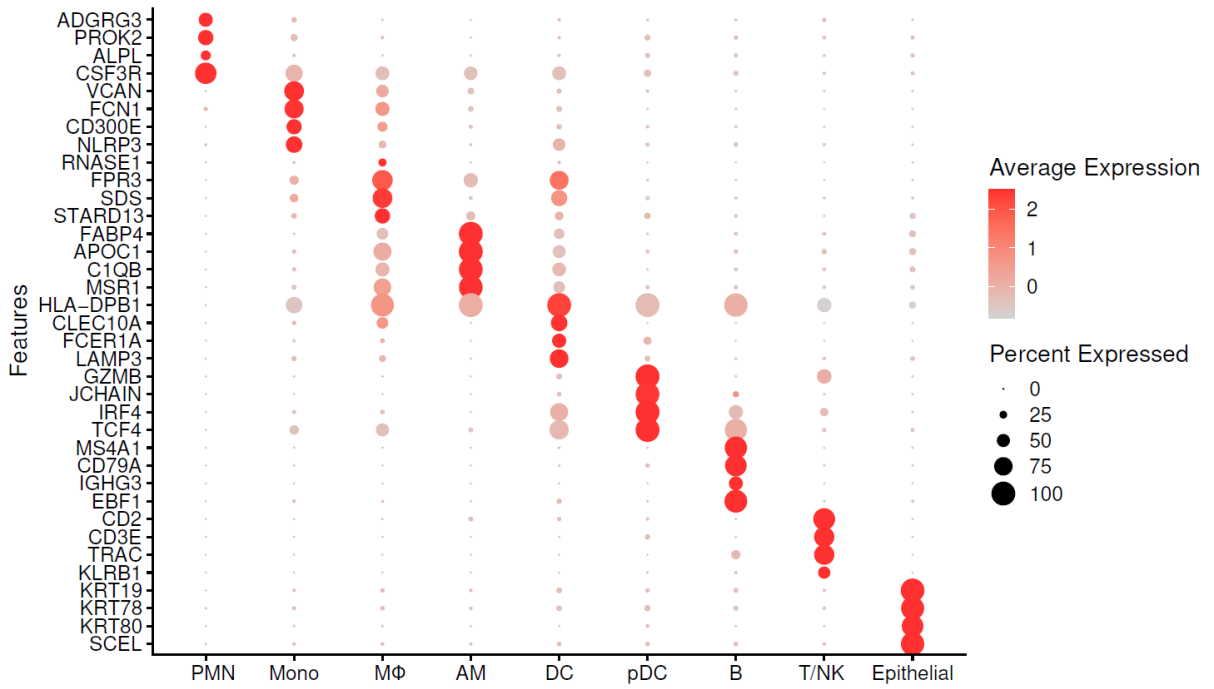

D

	CF_1	CF_16	CF_17	CF_18	CF_19	CF_2	CF_21	CF_22	CF_28	CTRL_23	CTRL_24	CTRL_25	CTRL_26	CTRL_5
AM	17	1	1	11	2	9	1	0	2	514	1758	1691	364	1769
B	25	52	113	10	17	48	96	22	60	44	5	17	14	19
DC	17	15	48	1	6	3	15	6	6	6	6	11	72	7
Epithelial	36	47	828	33	95	64	64	71	21	214	6	164	103	80
MΦ	29	20	48	3	8	10	23	1	27	43	90	105	214	35
Mono	166	549	227	137	281	426	420	56	69	4	5	3	14	34
PMN	1275	974	77	865	1103	1474	1526	177	471	12	6	12	82	34
pDC	1	21	26	0	36	0	6	1	2	3	1	0	2	1
T_NK	8	5	20	1	2	2	13	0	45	5	13	7	5	7

Figure S1: Human lung CCR2⁺ monocytes and macrophages are abundant in patients with CF. (A) Quantification of CCR2⁺ events / mm² of tissue from CCR2 stained human Non-CF and CF lung tissues. (B) Representative immunofluorescence staining for CCR2 (red), CD14 (yellow) and DAPI (blue) in CF human lung tissue. (C) Dot plot showing average expression and percent expression of marker genes used to identify sputum cell populations for scRNAseq studies. (D) Table showing the numbers of cells identified per cell cluster by scRNAseq for each individual sample. Related to **Fig. 1**.

Supplementary Figure S2

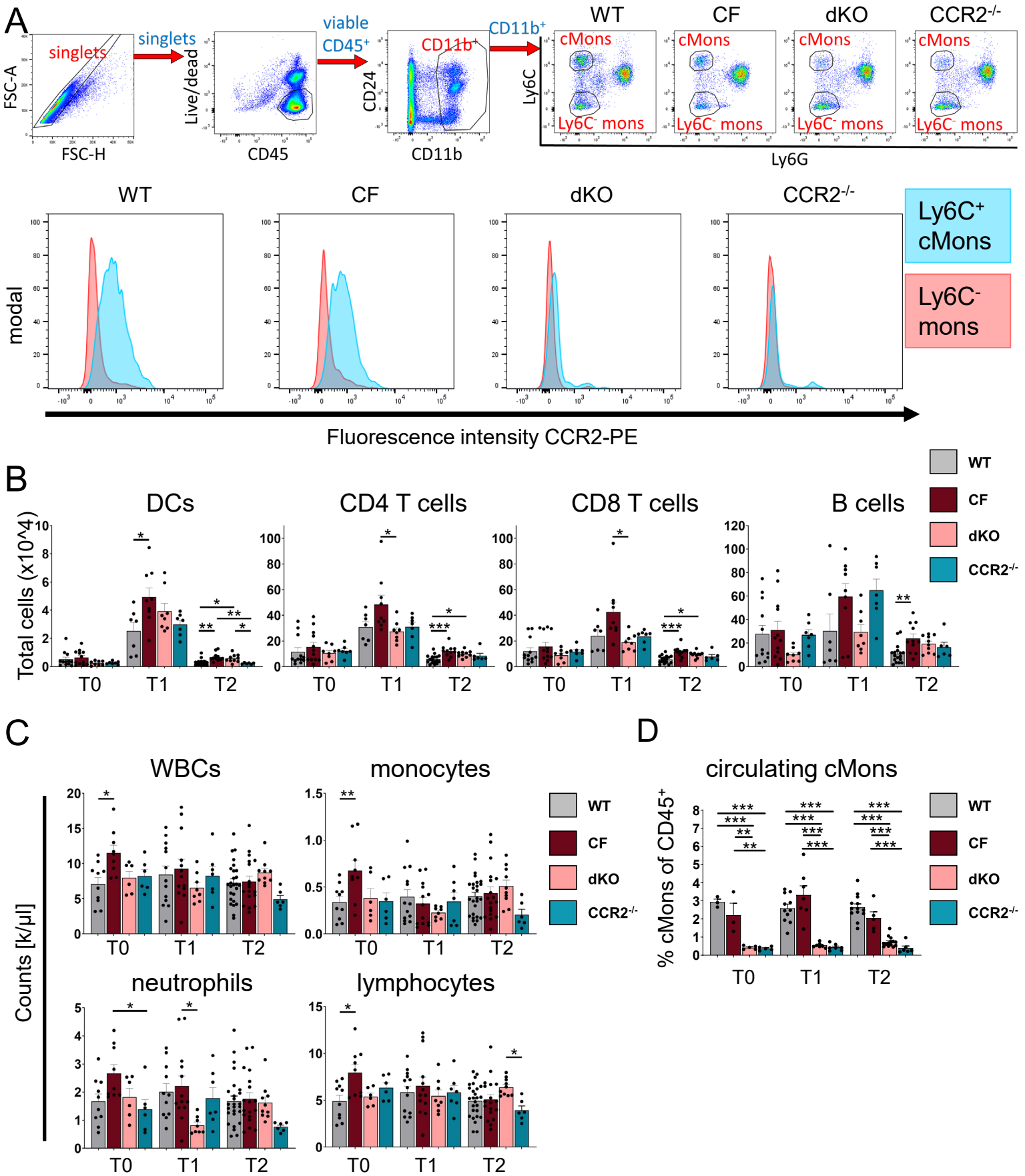

Figure S2: Characterization of immune cells in CF mouse models and CF patients. (A) Flow cytometry gating strategy of blood Ly6C$^+$ cMons and Ly6C$^-$ mons and histograms showing the fluorescence intensity of CCR2 staining in WT, CF, dKO, and CCR2$^{-/-}$ blood monocyte population (B) Total cell numbers of lung immune populations were quantified by flow cytometry as % of viable cells multiplied by lung cell count in the inferior lung lobe. (C) CBCs at T0, T1, and T2 of WT, CF, dKO, and CCR2$^{-/-}$ mice. (D) flow cytometry analysis showing the percentage of circulating cMons (CD11b$^+$Ly6C$^+$) among CD45$^+$ cells in blood. Data are generated form three independent experiments with n=2-6 mice per genotype and time point. Each biological replicate is represented by a dot. Bars are depicted as means ± SEM, significance was tested by One-way ANOVA and Tukey's multiple comparisons test between genotypes for each time point separately (* $p<0.05$; ** $p<0.01$; *** $p<0.001$). Related to **Fig. 2**.

Supplementary Figure S3

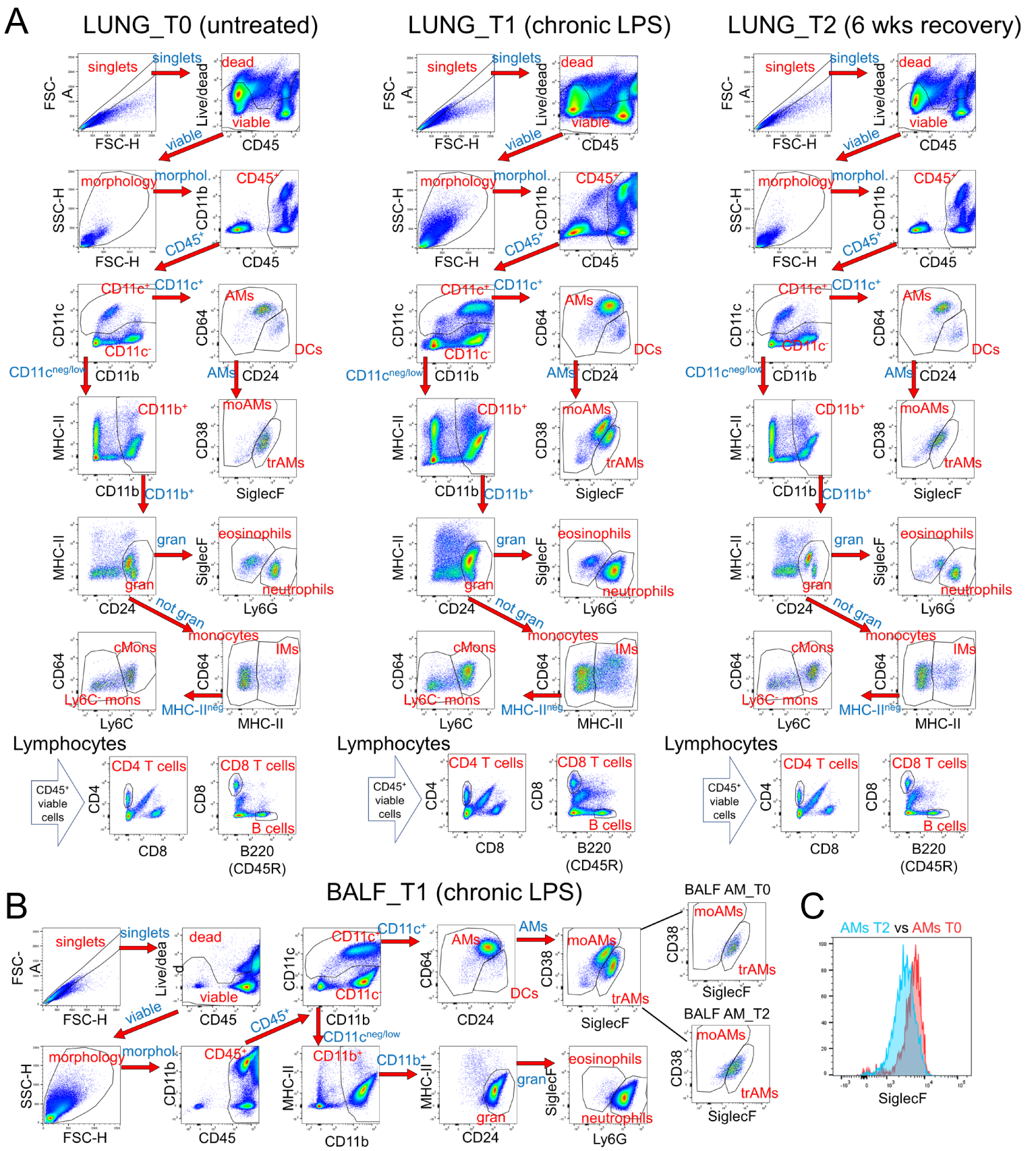

Figure S3: Flow cytometry gating strategy. Gating strategy on single lung tissue homogenates (A) and BALF (B) for assessed immune cells was adapted from Misharin et al 2013, see STAR methods for detailed description. (C) Histogram showing SiglecF expression in AMs at T0 and T2.

Supplementary Figure S4

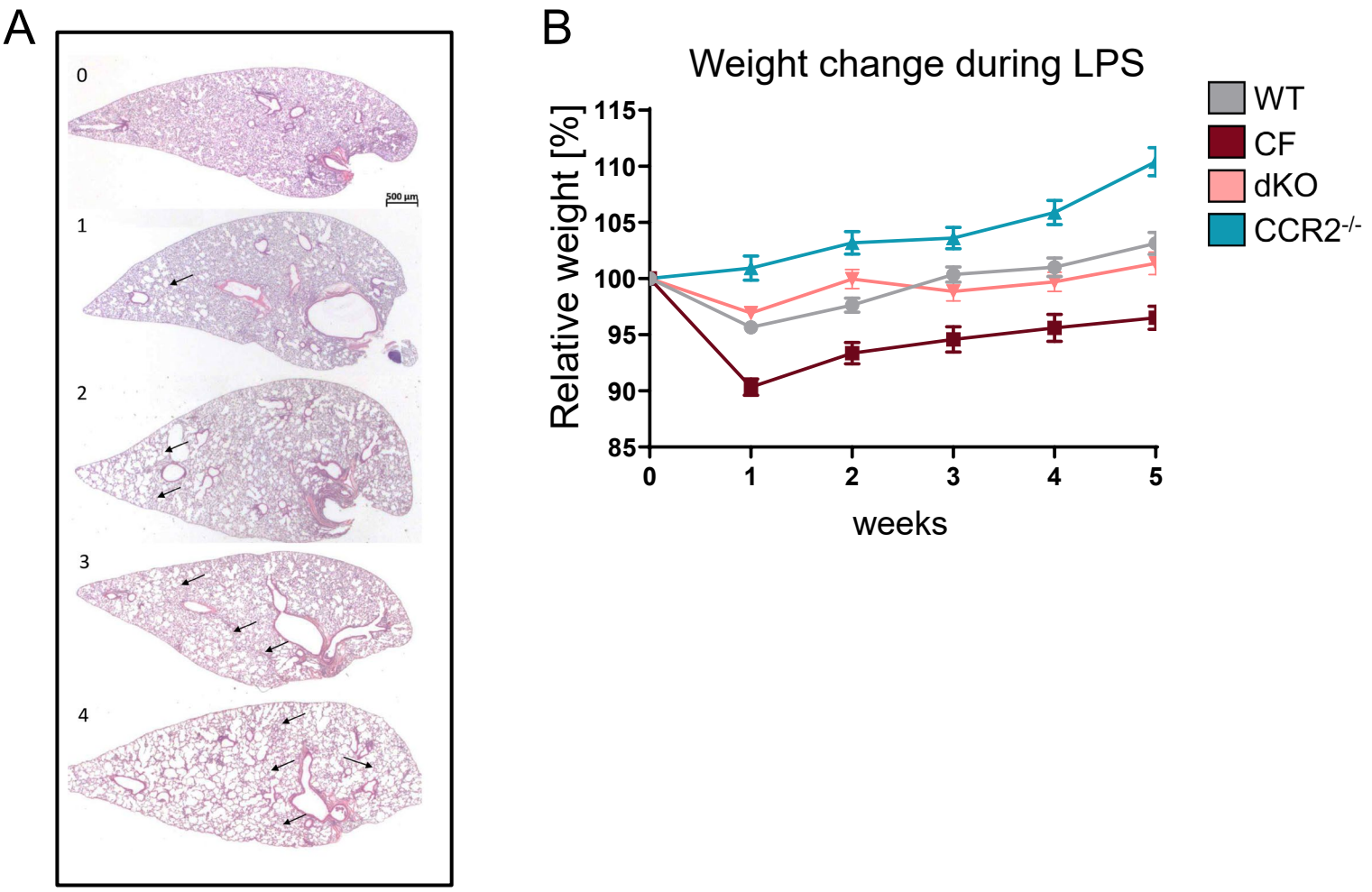

Figure S4: Weight loss and lung damage is limited by CCR2 deficiency (A) Alveolar architectural disruption scoring system: 0: Normal: homogeneous distribution of alveolar architecture throughout lung. 1: Mild: Alveolar expansion with septal disruption affecting <10% lung, typically apical (arrow). 2: Moderate: Alveolar expansion with septal disruption affecting 10-25% lung, typically apical (arrows). 3: Marked: Alveolar expansion with septal disruption affecting 25-50% lung, extending towards hilus (arrows). 4: Severe: Alveolar expansion with septal disruption affecting >50% lung, throughout (arrows). (B) Relative weight changes of WT, CF, dKO, and CCR2$^{-/-}$ mice during 5 weeks of LPS nebulization. Related to **Fig. 3**.

Supplementary Figure S5

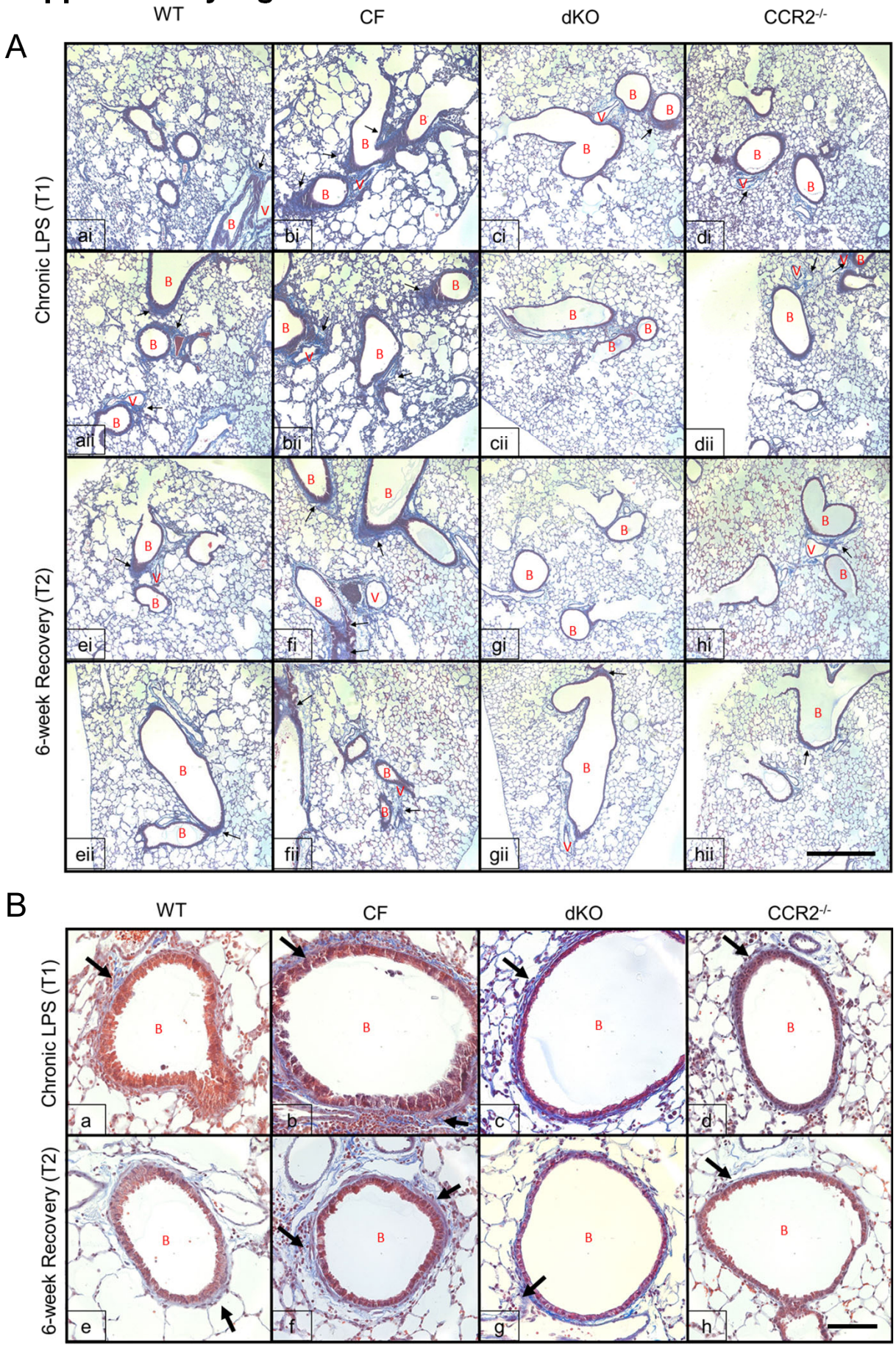

Figure S5: C**ollagen depositions are limited by CCR2 deficiency in CF mice.** The arrows indicate collagen deposition (blue), which were more abundantly accumulated at sites surrounding vascular vessels or bronchioles in samples from CF relative to WT, dKO, and CCR2$^{-/-}$ at 100x (A) and 400x (B) magnification. B, bronchioles; V, vascular vessels. Scale bar: (A) 500 μm; (B) 100 μm.

Supplementary Figure S6

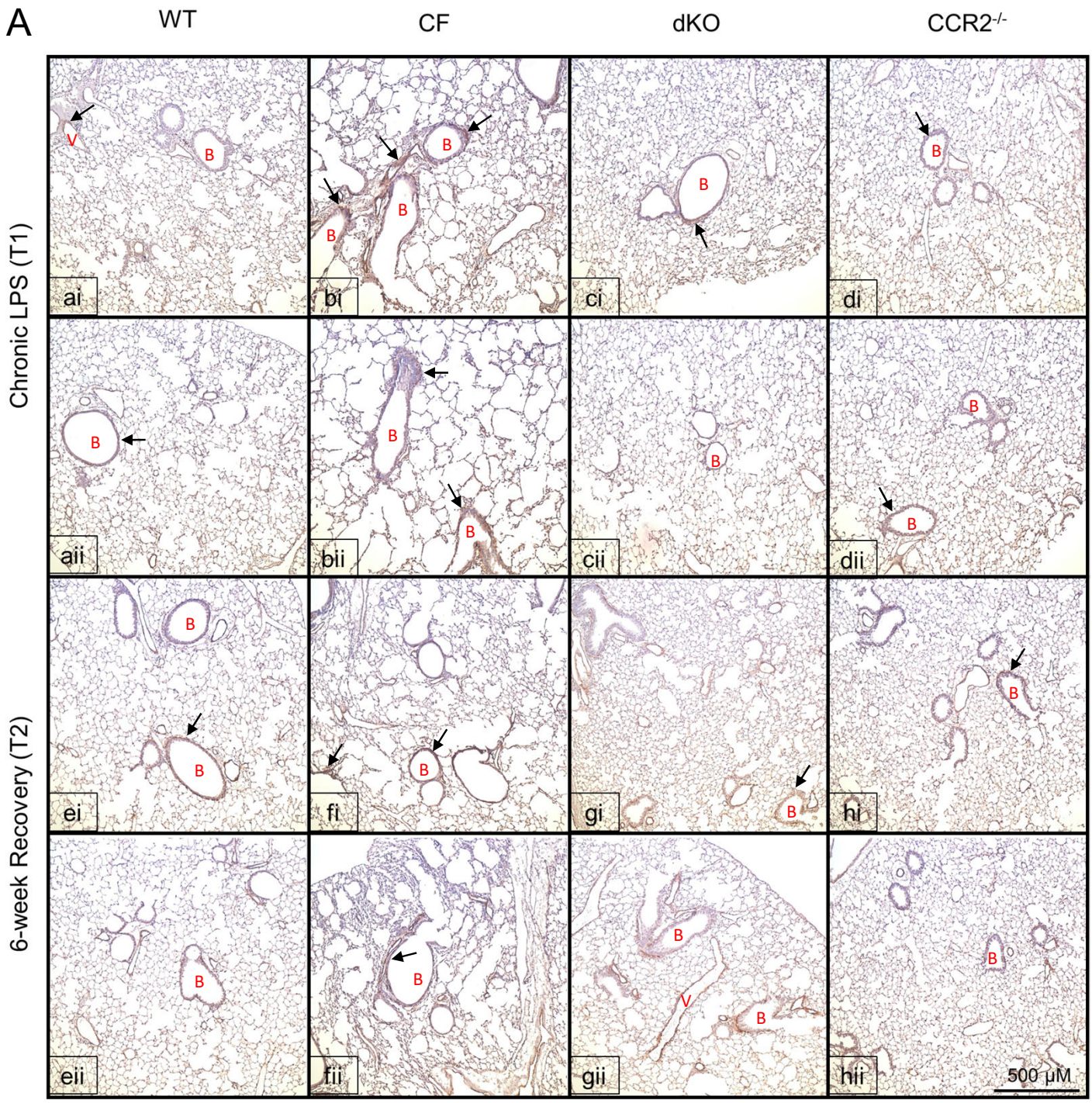

Figure S6: Myofibroblast accumulation is limited by CCR2 deficiency in CF mice. αSMA staining (dark brown), and hematoxylin staining of nuclei. The arrows indicate αSMA expression, which were more abundantly accumulated at sites surrounding vascular vessels or bronchioles in samples from CF relative to WT, dKO, and CCR2$^{-/-}$ at 100x magnification. B, bronchioles; V, vascular vessels. Scale bar: 500 μm.

Supplementary Figure S7

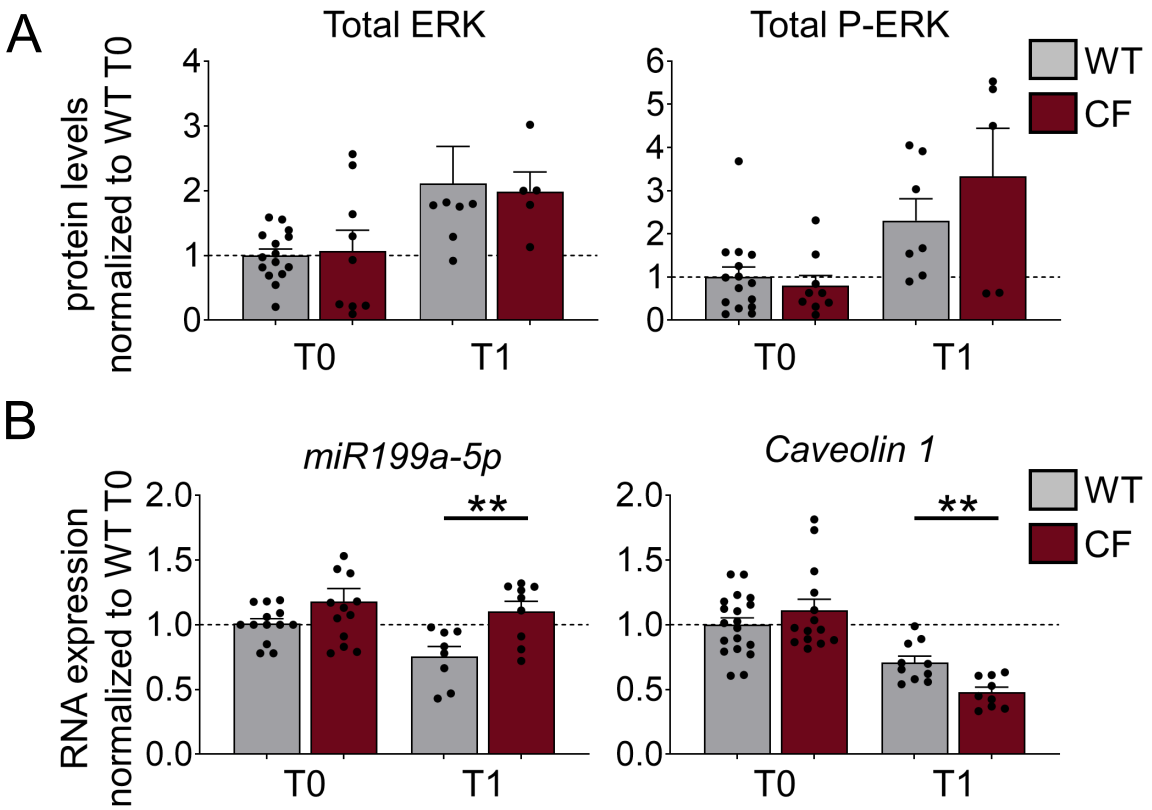

Figure S7: Additional TGFβ related signaling pathways. (A) Densitometric analysis of ERK and pERK in lung lysates of WT and CF mice at T0 and T1, normalized to *Vinculin* and WT T0. (B) *miR-199a-5p* (normalized to *Rnu6*) and *Caveolin1* (normalized to *18S*) RNA expression levels in lung lysates of WT and CF mice at T0 and T1 normalized to WT T0 levels. Bars are depicted as means ± SEM for n ≥ 6 mice per genotype and timepoint. Significance was tested by two-sided Student's t test between the genotypes for each time point separately (* p<0.05; ** p<0.01; *** p<0.001). Related to **Fig. 4**.

Supplementary Figure S8

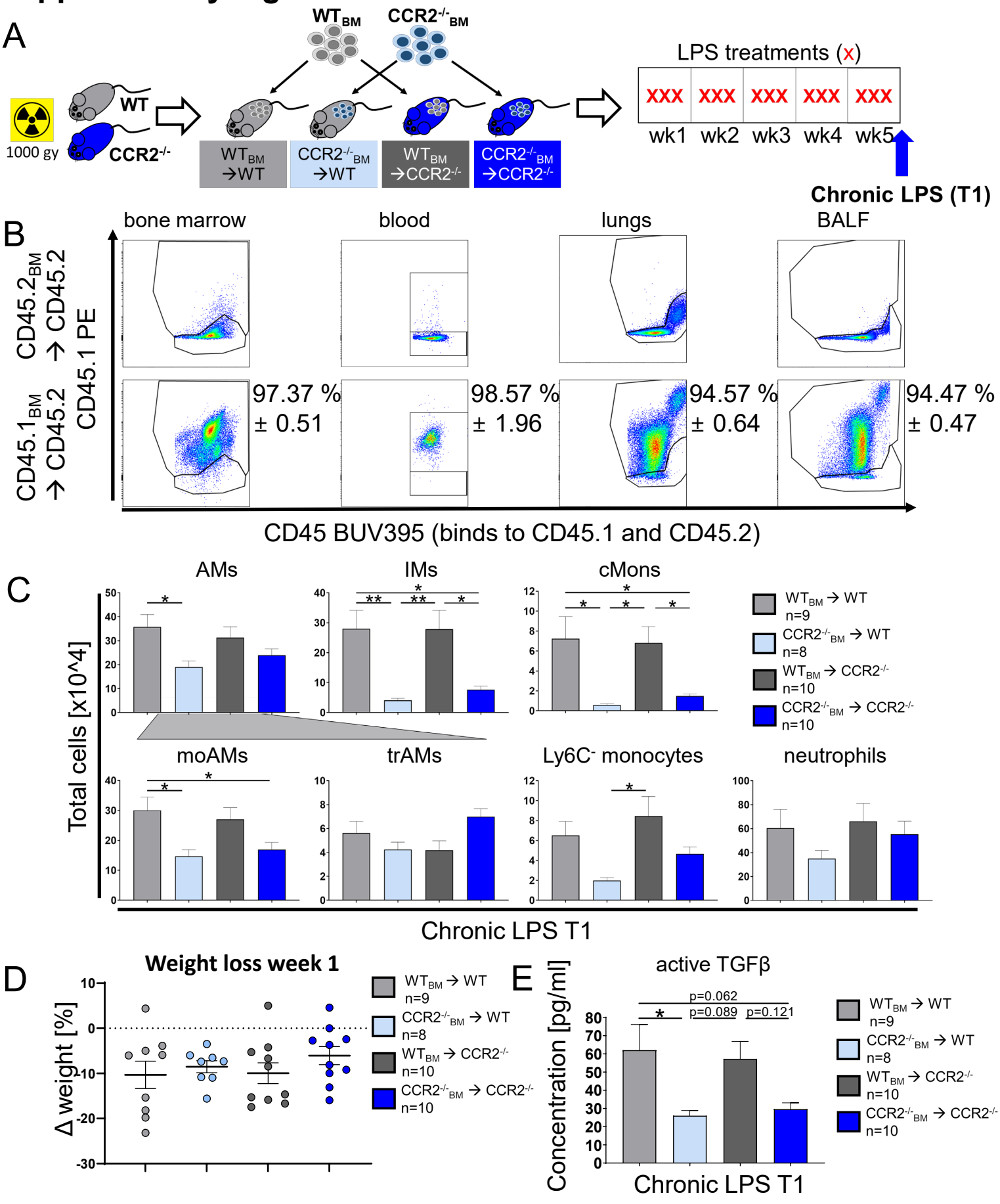

Figure S8: Bone Marrow Transplant model. (A) Adult WT and CCR2$^{-/-}$ mice were transplanted with bone marrow (BM) cells from WT or CCR2$^{-/-}$ mice. Six weeks after transplantation, mice were exposed to LPS for 5 weeks and sacrificed 24 h after the last nebulization (T1). (B) N = 3 WT host (CD45.2) mice receiving CD45.2 WT BM cells (top) or CD45.1 BM cells (bottom) were used to assess the indicated percentage of donor-derived CD45.1^{+} out of all CD45^{+} cells in BM, blood, lungs, and BALF at T1. (C) Quantification of immune cell numbers by FACS in the inferior lobe of transplanted mice at T1. (D) Relative weight loss after week 1 of LPS. (E) Active TGFβ levels in BALF of transplanted mice at T1 measured by ELISA. Data are generated form two independent experiments with n=4-5 mice per genotype. Each biological replicate is represented by a dot. Bars are depicted as means ± SEM, significance was tested by One-way ANOVA and Tukey's multiple comparisons test between genotypes for each time point separately (* p<0.05; ** p<0.01; *** p<0.001).

Supplementary Figure S9

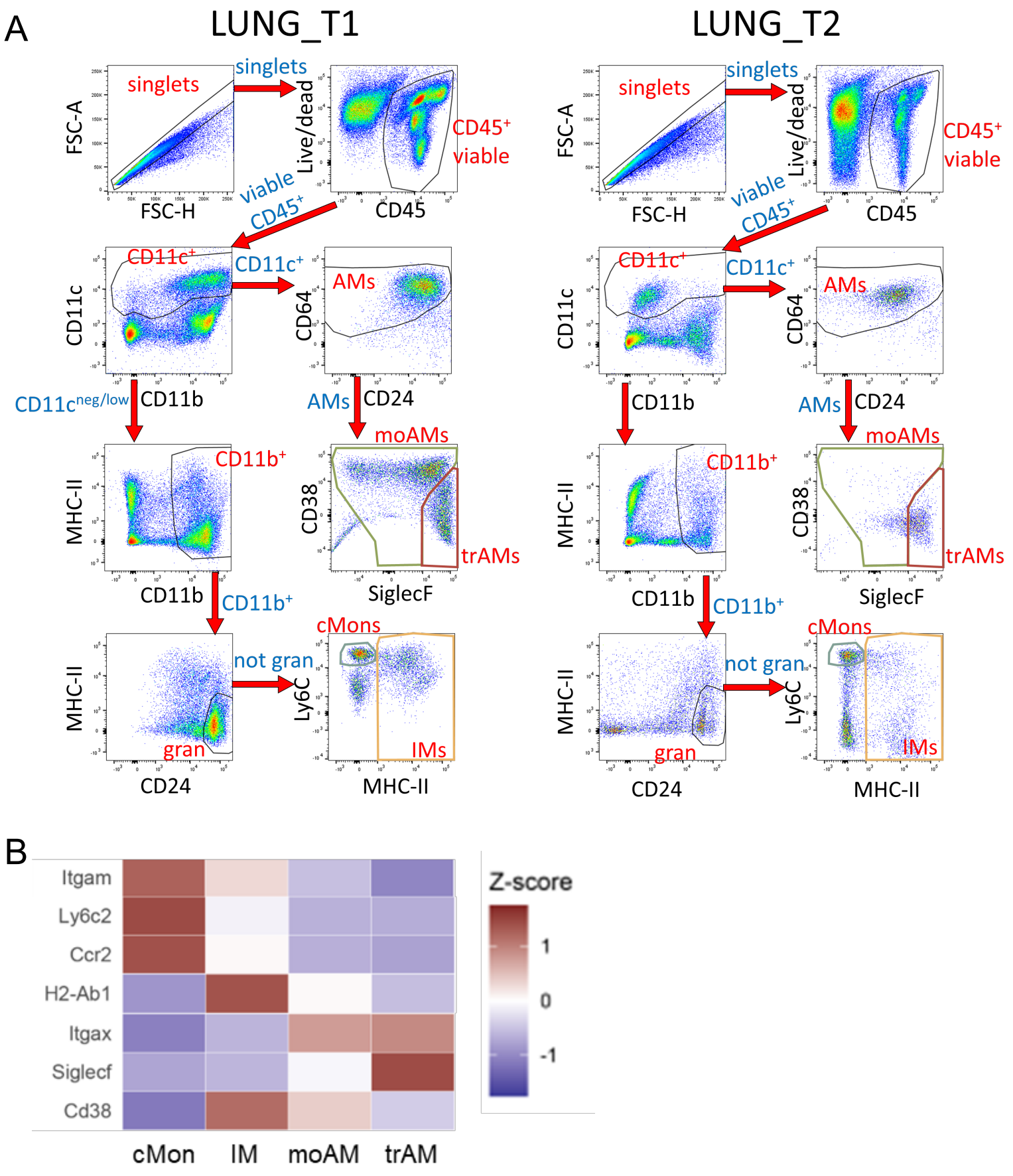

Supplementary Fig. S9: FACS gating strategy. (A) FACS gating strategy used to sort cMons, IMs, moAMs and trAMs from mouse lung tissue homogenates treated with LPS (T1) and after recovery (T2). Sorting gates are colored. (B) Heatmap from RNAseq analysis validating cellular markers that were used to identify and sort lung populations, independent of genotypes (WT and CF) and time points (T1 and T2). Related to **Fig. 5**.

Supplementary Figure S10

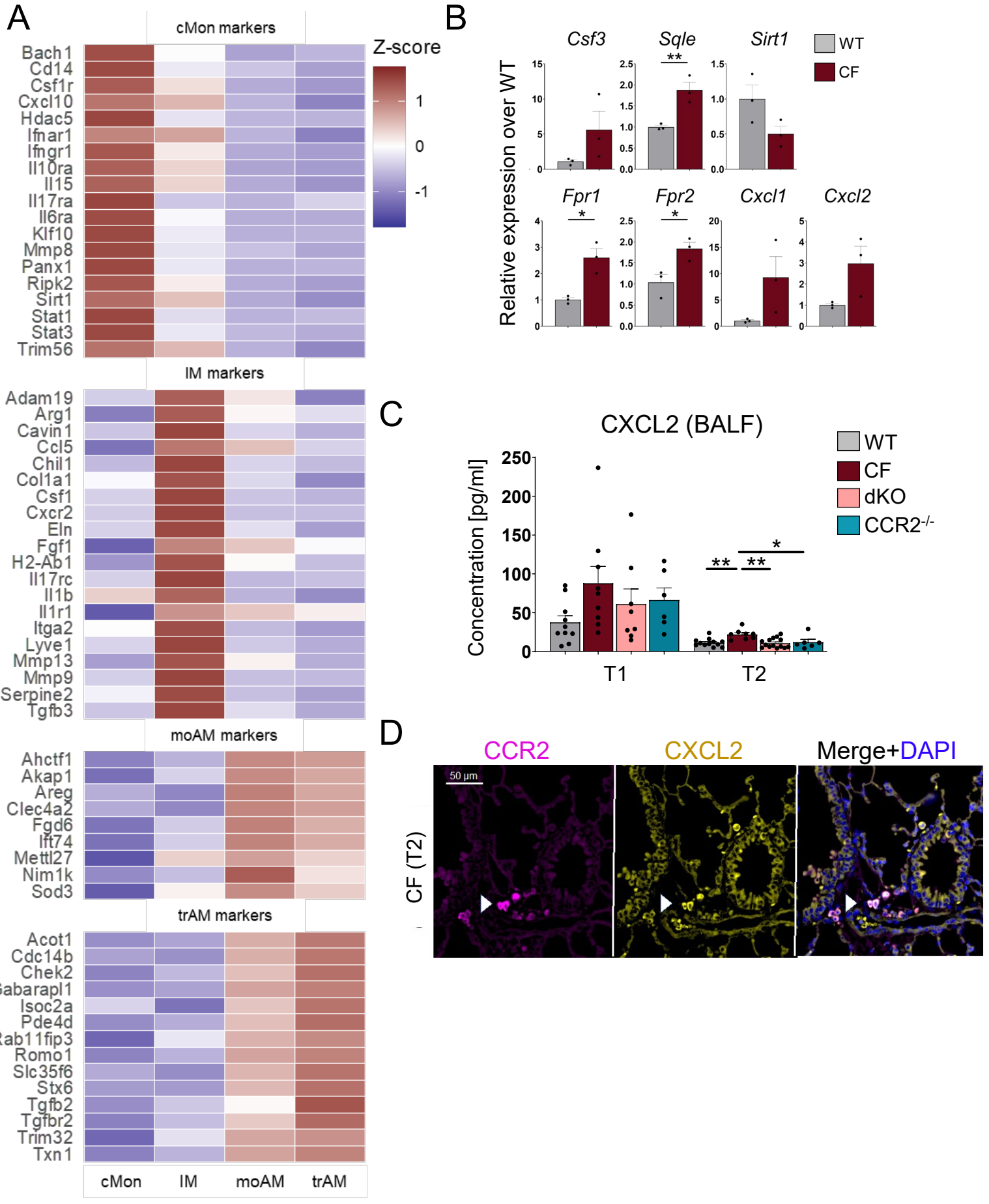

Figure S10. Characterization of WT and CF lung monocyte and macrophage transcriptome signatures. (A) Heatmap showing population markers associated with iMons, IMs, moAMs, and trAMs independent of genotypes (WT and CF) and time points (T1 and T2). (B) Validation of RNAseq data by qPCR for select DEGs comparing WT to CF cMons at T2 from n=3 biological replicates. (C) CXCL2 ELISA measured in BALF of WT, CF, dKO and CCR2$^{-/-}$ mice at T1 and T2. (D) IF staining of CF lung tissues at T2 stained for CCR2, CXCL2 and DAPI. White arrowheads indicate CCR2^{+}CXCL2^{+} cells. Related to **Fig. 5**.

Supplementary Figure S11

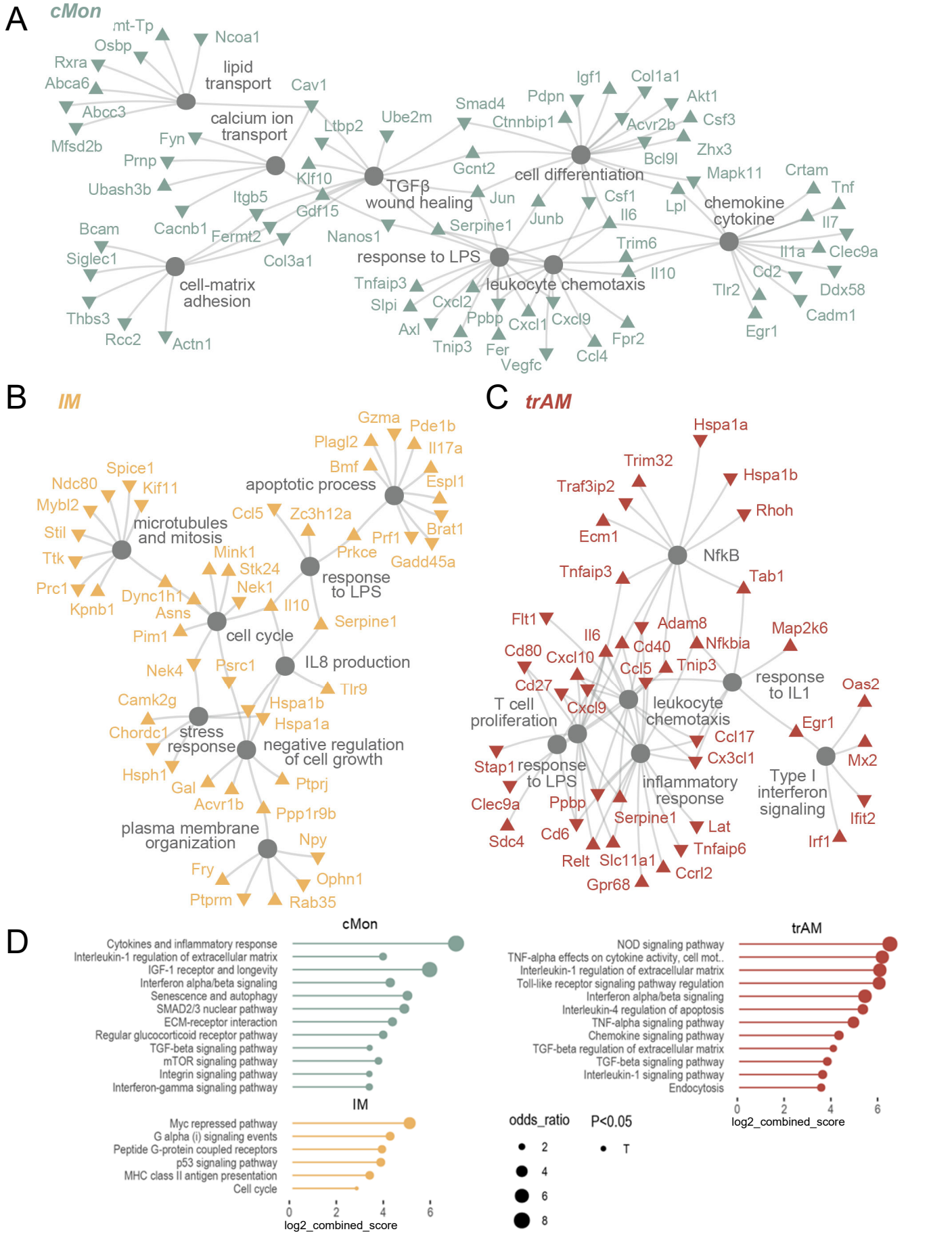

Figure S11. GO enrichment analysis of DEGs in CF between T1 and T2 compared to WT. One network was generated for each population (iMon (A), IM (B), trAM(C)). Genes upregulated and downregulated in CF are shown as arrowheads pointing up and down, respectively. Significantly enriched pathways associated with the genes are shown as closed circles (GO biological Process 2018). (D) BioPlanet_2019 enrichment analysis for genes differentially regulated in CF between T1 and T2 for cMons, IMs and trAMs. Node size: odds ratio associated with enrichment. P-value for Fisher's exact test. Related to **Fig. 5**.

Supplementary Figure S12

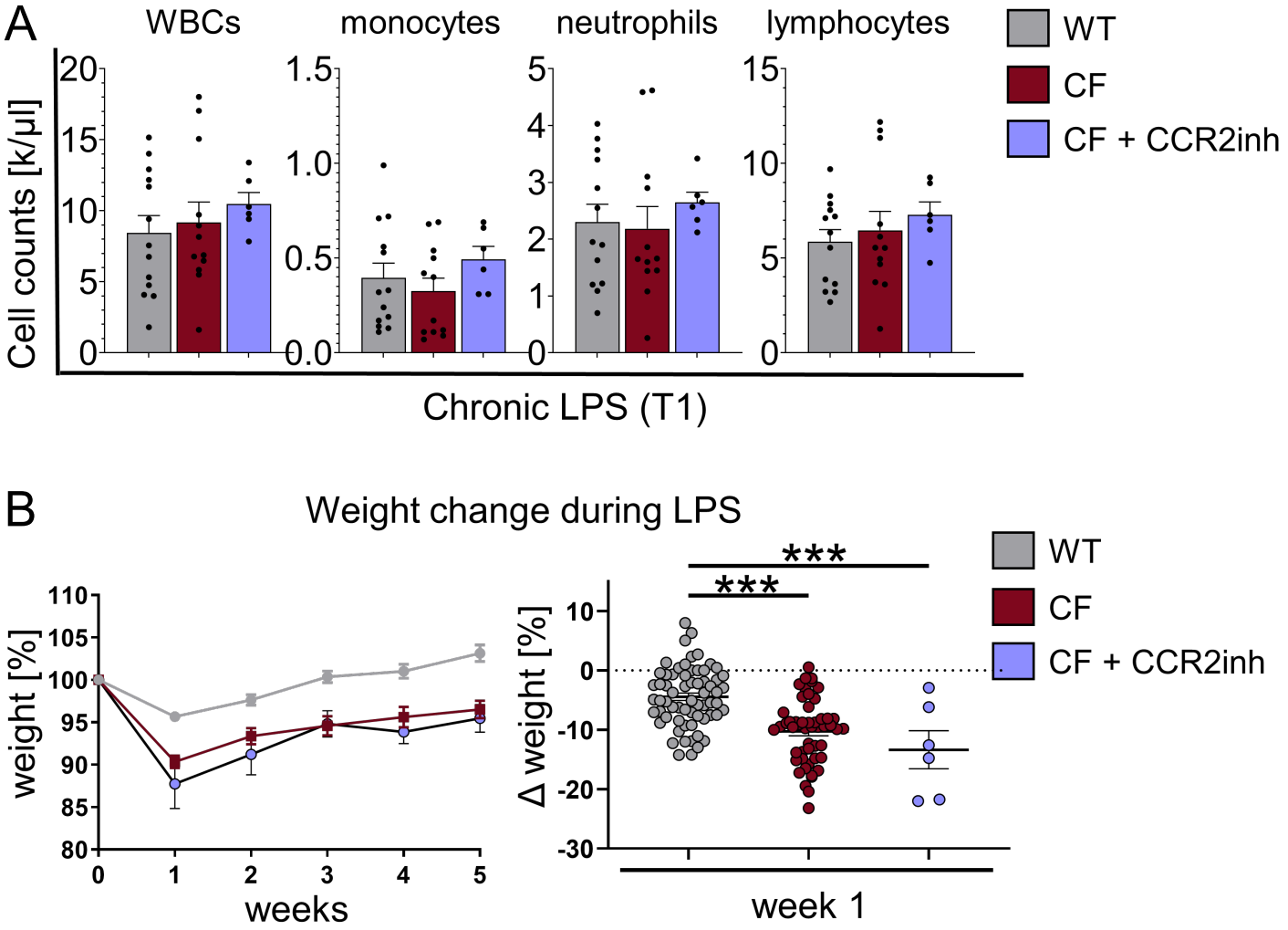

Figure S12. Supporting data for CF mice treated with CCR2 inhibitor. (A) CBCs in CCR2inh-treated mice at T0, T1, and T2. (B) Weight loss during 5 weeks of chronic LPS (left) anthreed after week 1 of LPS (right) for WT, CF, and CF + CCR2inh mice. Each biological replicate per genotype and experimental condition is represented by a dot. Bars are depicted as means ± SEM, significance was tested by One-way ANOVA and Tukey's multiple comparisons test between genotypes for each time point separately (* p<0.05; ** p<0.01; *** p<0.001). Related to **Fig. 7**.

Supplementary Figure S13

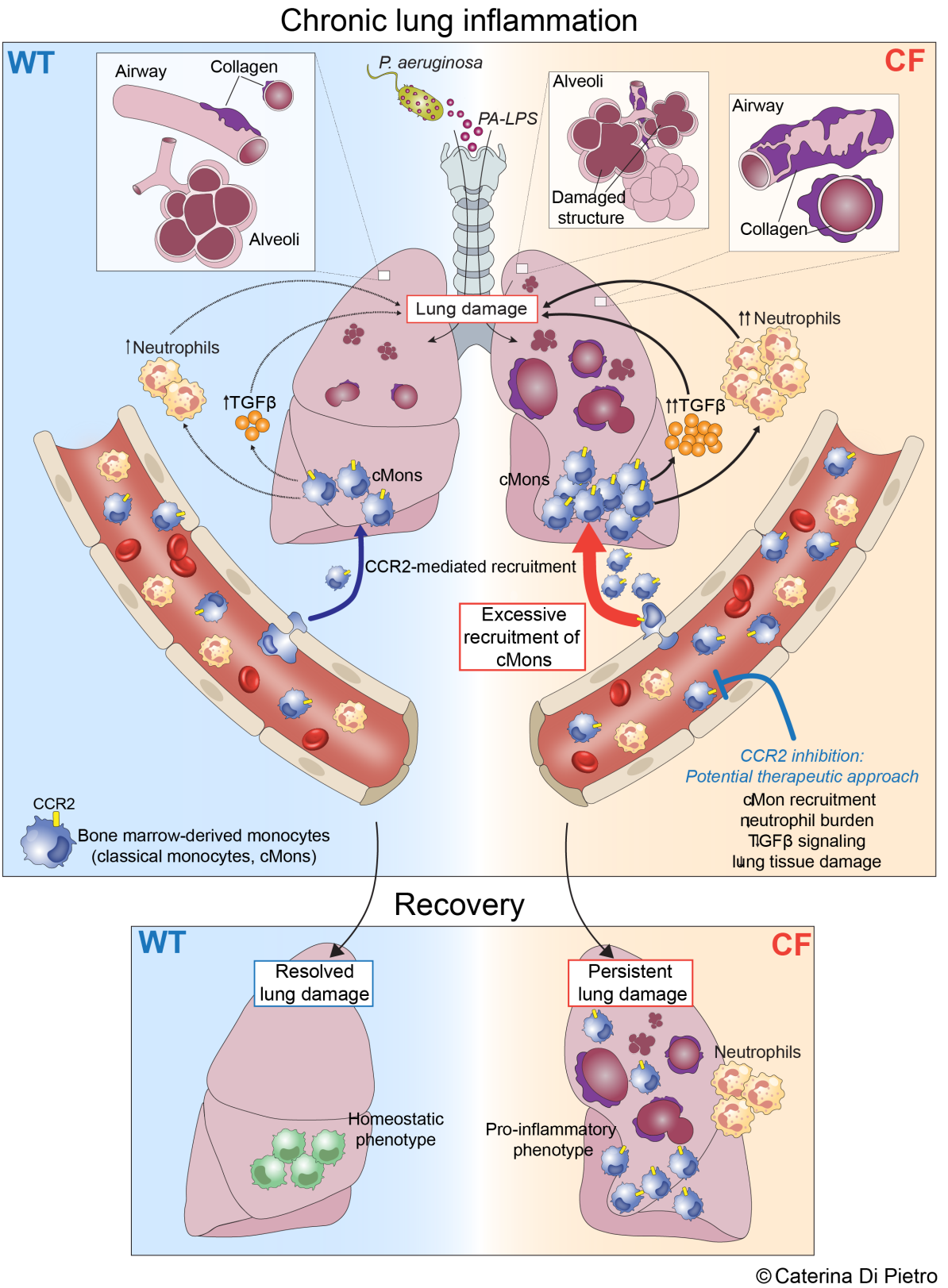

Figure S13: Working model. Inflammatory triggers lead to excessive accumulation of CCR2+ classical monocytes in lungs of cystic fibrosis (CF) patients and mice. These sustain a pro-inflammatory phenotype, drive pathogenic TGFβ signaling, facilitate neutrophil recruitment, and cause persistent lung damage. Targeting their recruitment via CCR2 inhibition is a potential target to ameliorate lung tissue damage in CF.

Supplementary Table S1: Patient demographics

Definition of abbreviations: BMI = body mass index; CF = cystic fibrosis; CFTR= cystic fibrosis transmembrane conductance regulator; HC = healthy control; NA = not applicable; P. aeruginosa = Pseudomonas aeruginosa.

Characteristics	HC Subjects (*n* = *5*)	Subjects with CF (*n* = *9*)
Age, yr		
Mean ± SD	35.4 ± 5.9	30.6 ± 6.5
Range	26–42	24–43
Sex, *n* (%)		
F	2 (40)	6 (67)
M	3 (60)	3 (33)
Mutation background, *n* (%)		
F508del/F508del	NA	7 (77.8)
F508del/other	NA	2 (22.2)
No *F508del* mutations	NA	0 (0)
FEV_1, L		
Mean ± SD	NA	1.9 ± 0.7
Range	NA	0.68–2.85
FEV_1, %		
Mean ± SD	NA	57 ± 21.5
Range	NA	19–84
BMI, kg/m^2		
Mean ± SD	NA	22.2 ± 2.1
Range	NA	19.11–25.73
CF comorbidities, *n* (%)		
Pancreatic exocrine insufficiency	NA	9 (100)
CF-related diabetes	NA	4 (44.4)
Liver disease	NA	1 (11.1)
Microbiology, *n* (%)		
P. aeruginosa colonization	NA	5 (55.6)
CFTR modulators, *n* (%)		
Ivacaftor/tezacaftor	NA	6 (66.7)